

C₂ Swan band laser-induced fluorescence and chemiluminescence in low-pressure hydrocarbon flames

Gregory P. Smith^{*}, Chung Park, Justin Schneiderman¹, Jorge Luque²

Molecular Physics Laboratory, SRI International, Menlo Park, CA 94025, USA

Received 24 June 2004; received in revised form 29 November 2004; accepted 26 December 2004

Available online 2 February 2005

Abstract

Laser-induced fluorescence from the excitation of the C₂(*d-a*) 2, 0 band at 438 nm is used to determine spatial profiles and relative lower state concentrations in several low-pressure hydrocarbon–air premixed flames, to determine the fuel-rich flame kinetics. Quenching loss rate constants are derived from the measured fluorescence decay rates. Quantitative Swan band chemiluminescence intensities, coupled with computer modeling of the flame kinetics and excited state loss rates, lead to recommended values of rate constants for the excited C₂(*d*)-state chemiluminescence production kinetics.

© 2005 The Combustion Institute. Published by Elsevier Inc. All rights reserved.

Keywords: Chemiluminescence; C₂; LIF; Low-pressure flames

1. Introduction

The blue-green Swan band emissions are a prominent visible feature in many flames [1], and form one of the oldest observed and assigned molecular electronic spectra [2]. The system also shares great astronomical significance, forming the famous comet bands [3,4]. The spectroscopic lines, constants, intensities, and lifetimes have been studied [5]. This transition is used in combustion studies that report measurements of chemiluminescent emission and laser-induced fluorescence (LIF). We have recently reexamined [6] visible flame luminescence—OH(A²Σ⁺-

X²Π) at 310 nm, CH(A²Δ-X²Π) at 430 nm, and here C₂(*d*³Π-a³Π)—as a useful diagnostic for applications where more complex laser methods are inconvenient, such as under microgravity conditions. A quantitative analysis of such measurements with a chemical kinetics interpretation requires knowledge of the excited state production and loss reaction rates. In this work we directly measure the C₂(*d*) loss rate by examining the decay of C₂(*d-a*) laser-induced fluorescence. Previous observations of Swan band chemiluminescence in the same flames provided excited state concentrations [6]; with the new decay rates, production rate constants are derived that can be used to model this signature. Potential uses for Swan band emission diagnostics lie in rich or sooting hot local environments, and can perhaps be extended to interpret signals in laser-induced incandescence [7], or as a flame stoichiometry sensor [8].

The quantitative application of C₂(*d-a*) laser-induced fluorescence as a diagnostic tool is addressed

^{*} Corresponding author. Fax: +1-650-859-6196.

E-mail address: gregory.smith@sri.com (G.P. Smith).

¹ Current address: Physics Department, University of Southern California, Los Angeles, CA, USA.

² Current address: Lam Research Corporation, Fremont, CA 94538, USA.

by the present experiments. Decay rate measurements provide direct values for the fluorescence quantum yield under flame conditions, which is a necessity for absolute LIF concentration determination. Very few quenching rates are available, even at room temperature. Our values form a basis for making estimates in other flames. LIF diagnostics experiments in the well-controlled environment of a low-pressure premixed laminar flame have spatial, spectral, and temporal resolution that allows us to follow the evolving flame chemistry; these observations help in the design of combustion LIF diagnostics. $C_2(d-a)$ LIF has been used previously in flames [9–11], and quantitative LIF measurements in high-temperature diamond-depositing plasma reactors were performed [12–16]. Chemiluminescence was also investigated in both environments. A recent experiment has determined absolute $C_2(a)$ concentrations in diffusion flames using cavity ringdown absorption spectroscopy (CRDS) and LIF of the Swan bands [17]. CRDS has also been used to measure $C_2(A^1\Pi)$ state concentrations in an oxyacetylene flame [18].

Finally, chemical mechanisms can be tested using C_2 LIF measurements and C_2 models in fuel-rich or near-sooting flames, as C_2 is closely related to acetylene, which is a known soot precursor. C_2 measurements are also useful to the development of CH(A-X) chemiluminescence diagnostic techniques. The reactions of $C_2H + O$ or O_2 are the likely important CH(A) sources, and the C_2H concentration is related to C_2 via $C_2 + H_2 \leftrightarrow C_2H + H$. So if a model properly simulates the C_2 LIF measurements, it is likely to properly predict the C_2H precursor and provide a sensitive assessment of the CH(A) production rate constant.

The source reactions for $C_2(d-a)$ emission are not certain. Appearance of these emissions in rich flames or regions provides an argument against [1, 19] possible exothermic O atom reactions such as $O + C_3 \rightarrow CO + C_2(d)$ as the primary source. The isotope work of Ferguson [20] in acetylene flames suggests that reactions of two separate single-carbon-atom species are responsible, and disfavors steps in which the fuel CC bond is preserved in the emitter. Candidates include $C + CH$, $CH + CH$, and $C + CH_2$. It is difficult to distinguish the importance of each of these steps from premixed low-pressure flame data, because of the proximate locations and kinetic correlations of the CH_x species. But for the same reasons, it may not matter operationally. Measurements of CH and Swan band emissions in acetylene flames by Bulewicz et al. [21] provide an argument against the $CH + CH$ reaction. A recent flow reactor study [22] showed that more C_2H^* chemiluminescence occurs than $C_2(d-a)$ emission. An earlier study [23] of the timing of light emissions from shock-heated methane

favors the $C + CH$ (or CH_2) reaction and not $CH + CH$ as the Swan band source. A flow discharge examination [19] of the kinetics in the $C_2H_2/O/H$ system supports $C + CH_2$ as the main production step. Two other exothermic reactions mentioned in the literature also merit consideration as possible Swan band sources. Savadatti and Broida [24] observed $C_2(d-a)$ emissions in atomic carbon flames in oxygen, particularly with atomic oxygen, which suggests the reaction $O + C_3 \rightarrow CO + C_2(d)$ occurs. There are reports [25] that vibrationally excited $C_2(d)$ is produced at high pressure by the reaction $C + C_2O \rightarrow C_2(d, v' = 6) + CO$.

Prior information about the quenching of excited state $C_2(d)$ is very limited, even at room temperature. One high-temperature quenching rate was determined in an arc jet mixture of Ar, H_2 , and H [14]. Room temperature data can be found for Xe, C_2H_2 , C_2H_4 , and O_2 [10,26–28]. Generally, rapid rates were found.

This study reports spatial profiles of $C_2(d)$ and $C_2(a)$ measured in five low-pressure laminar flat premixed flames with methane, ethane, and ethylene fuels. $C_2(d)$ was measured at various heights above the burner by CCD imaging the Swan band emission in a system that was previously calibrated using Rayleigh scattering, and subsequent Abel inversion. Relative $C_2(a)$ was measured at various heights using $C_2(d-a)$ LIF. The excited state quenching loss rates were determined from the decay of the time-resolved LIF signal. The time decay information is needed to make the concentration profiles quantitative. Absolute d -state and relative a -state concentrations were derived for the flames. Modeling calculations of these flames were performed to interpret the results, with the goals of validating our understanding of C_2 kinetics and deriving accurate rate constants for $C_2(d)$ production and quenching in hydrocarbon–air flames.

2. Experimental

Conditions characterizing the five premixed hydrocarbon–air flames studied here are summarized in Table 1. The rich methane flame was featured in our previous LIF studies of methane flame chemistry [29]. Details of the experiments, temperature distributions from OH LIF rotational excitation scans, and absolute CH profiles versus height above the burner may be found in that work. Chemiluminescence results for this flame and details of those experiments have been presented [6], but full analysis of the $C_2(d-a)$ results requires the current quenching measurements. Temperatures for the new ethane and ethylene flames were measured with our standard method [29], by LIF of OH rotational levels using 14 lines of the R branch of the (0, 0) transition near 307 nm, and the temperature profile was fit to the empirical four-parameter expres-

Table 1
Flame conditions

Fuel	Φ	P (Torr)	Fuel flow (slm)	O ₂ flow (slm)	N ₂ flow (slm)	A	B	C	D	T^a at C ₂ max (K)
Methane	1.28	30	0.78	1.22	2.78	669	1357	−0.094	2.052	1930
Ethane	1.02	25	0.25	0.84	1.93	348	1545	−0.331	1.225	1670
Ethane	1.28	30	0.31	0.84	1.93	404	1590	−0.381	1.148	1730
Ethylene	1.02	25	0.29	0.84	1.93	409	1384	−0.452	1.136	1540
Ethylene	1.28	30	0.36	0.84	1.93	403	1574	−0.553	0.991	1700

^a $T = A + B[1 - \exp(-Ch^D)]$, with height h in mm.

sion shown. The last column of Table 1 gives the flame temperature at the height of maximum C₂(a) concentration. We also performed some chemiluminescence intensity measurements in our 25-Torr near-stoichiometric methane–air flame ($\Phi = 1.07$) [29].

Operation at low pressure allows good spatial resolution of the flame structure of each species, and thus the progress of the flame chemistry can be followed, via LIF or chemiluminescence. The flames are supported on a 6-cm-diameter sintered plug McKenna burner, housed inside a vacuum chamber designed for optical probing. A concentric flow of argon is used to isolate and stabilize the flame. The burner translates vertically with respect to the optical axis of the laser and the detection system. A servo control valve maintains the chamber and flame pressure, while mass flow controllers regulate the fuel, oxygen, and nitrogen. A laser beam traverses the chamber through Brewster angle windows, with power monitored at the exit (Laser Precision Rj-7200), for the LIF measurements. A large silica window, through which light may be imaged onto either spectrometer or filtered CCD camera detection systems, lies perpendicular to the laser path. These are the detection setups for LIF and chemiluminescence, respectively.

The C₂(d) concentrations and distributions were measured, as in the prior work [6], by imaging the flame emissions through a long-pass filter (>450 nm, Schott GG455) onto a gated intensified CCD camera operating in simple shutter mode (Princeton Instruments, ICCD 576G.RBT, 14 bits dynamic range, 384 × 576 pixels). Pixel resolution is 0.0187 cm. An Abel inversion is performed to deconvolute the line-of-sight integrated signal, and determine flame-center excited state concentration height profiles from the computer-stored two-dimensional images. Absolute amounts are obtained by comparison with the previously measured rich methane flame values [6]. The original calibration used Rayleigh scattering of a 430-nm laser intensity by nitrogen densities to determine the absolute sensitivity of the optical detection system and thus the absolute concentration of flame CH(A) emitters [6,30,31]. A standard lamp was used for rel-

ative sensitivity determinations at the other chemiluminescence wavelengths and optical filters.

The C₂($d-a$) LIF was excited at the (2, 0) bandhead by 438.2-nm light from a Lambda Physik FL-2002 dye laser pumped by an EMG103 excimer laser, using the dye Coumarin 120, at 10 Hz. The (3, 1) band at 437.1 nm was also examined. The laser energy levels of 10–50 μJ begin to saturate the strong transition. The 10-ns-duration pulses had a bandwidth of 0.24 cm^{−1}, as determined from a nearby CH(A-X) LIF excitation linewidth in a spectrum measured under linear excitation conditions. Fluorescence at right angles to the laser beam was focused into a Bausch and Lomb 0.25-m monochromator, featuring a 20-nm bandpass typically centered at 473 nm near the $\Delta v = 1$ origin for the maximum signal, and onto a 1P28 photomultiplier. Signals were processed by an SRS boxcar averager (20 shot average, 100-ns-wide prompt gate) for excitation spectra and burner height scans, and a digitizing oscilloscope (Tektronix TDS350, 500 shot average) for fluorescence lifetimes, under computer control via Labview programs. While LIF height profiles were being taken, a second boxcar set to dc-average the flame emission signal at a delay after the laser was used to obtain C₂(d) excited state profiles (chemiluminescence integrated along the line of sight). The peak of this spatially integrated profile is 0.2–0.4 mm higher than the Abel inverted center-line distribution, and has a tail to larger heights. These results served to confirm the relative flame intensities of the Swan band emission CCD experiments.

We performed one-dimensional flame model calculations using the Sandia code PREMIX [32] for flat laminar flames with transport and the GRI-Mech 3.0 chemical mechanism for methane oxidation [33]. Measured flow rates and temperature profiles are also inputs. The flat radial distributions of chemiluminescence from the Abel inversions [6] suggest the one-dimensional modeling approximation is reasonable. A few reactions involving C and C₂ species were added, beyond the requirements of GRI-Mech; they were included and described in the previous chemiluminescence study [6], as trace species involved in the production kinetics relating to CH(A-X) chemi-

Table 2

Additional C₂ kinetics: $k = AT^n e^{(-E/RT)}$

Reaction	A (cm ³ /mol/s)	n	E (cal/mol)	Source
Reactions added to GRI-Mech 3.0 for all models				
C ₂ + H ₂ = C ₂ H + H	4.0e5	2.4	1000.	[6]
CH + CH = C ₂ + H ₂	5.0e12	0	0	[6]
C + C + M = C ₂ + M	3.0e14	0	–1000.	[6]
C + CH = C ₂ + H	5.0e13	0	0	[6]
O + C ₂ = C + CO	5.0e13	0	0	[6]
C ₂ + O ₂ = CO + CO	9.0e12	0	980.	[38]
Reactions involving C₂[*]				
C ₂ [*] ⇒ C ₂	1.0e7	0	0	[34,35]
C ₂ [*] + M = C ₂ + M	4.8e13	0	0	This work
C + CH ₂ ⇒ C ₂ [*] + H ₂	2.4e12	0	0	This work 1/2 model B
O + C ₃ ⇒ CO + C ₂ [*]	4.2e11	0	0	This work model C
Added reactions for Model C				
C + C ₂ H ₂ = C ₃ H + H	1.2e14	0.	0.	[42]
C + C ₂ H = C ₃ + H	2.0e16	–1.0	0.	est.
CH + C ₂ H ₂ = C ₃ H ₂ + H	9.36e13	0.	–500.	[43]
CH + C ₂ H = C ₃ H + H	5.0e13	0.	0.	est.
CH + C ₂ = C ₃ + H	5.0e13	0.	0.	est.
C ₃ + H ₂ = C ₃ H + H	4.0e5	2.4	22000.	est. (endothermic)
C ₃ H + H ₂ = C ₃ H ₂ + H	4.0e5	2.4	1000.	est. (C ₂ H + H ₂)
H + C ₃ + M = C ₃ H + M	2.44E+32	–4.8	1900.	est. $k(\text{inf}) = 1e17/T$
H + C ₃ H + M = C ₃ H ₂ + M	1.66E+33	–4.8	1900.	est. $k(\text{inf}) = 1e17/T$
O + C ₃ = CO + C ₂	5.0e13	0.	0.	est.
OH + C ₃ = CO + C ₂ H	2.0e13	0.	0.	est.
O ₂ + C ₃ = CO ₂ + C ₂	9.0e12	0.	11000.	[45], est. (C ₂ + O ₂)
O + C ₃ H = CO + C ₂ H	4.0e13	0.	0.	est.
OH + C ₃ H = CO + C ₂ H ₂	2.0e13	0.	0.	est.
O ₂ + C ₃ H = CO + HCCO	3.0e13	0.	0.	est. (C ₂ H + O ₂)
O + C ₃ H ₂ = HCO + C ₂ H	4.0e13	0.	0.	est.
OH + C ₃ H ₂ = HCO + C ₂ H ₂	1.0e13	0.	0.	est.
CH + CO = H + C ₂ O	4.4e11	0.	5200.	[45], NIST ^a rev.
OH + HCCO = H ₂ O + C ₂ O	3.0e13	0.	0.	est.
O + C ₂ O = 2CO	5.0e13	0.	0.	[46]
OH + C ₂ O ⇒ H + 2CO	2.0e13	0.	0.	est.
O ₂ + C ₂ O = CO + CO ₂	2.0e13	0.	2700.	NIST
H ₂ + C ₂ O = CH ₂ + CO	4.0e13	0.	2300.	est.
OH + C ₂ = C ₂ O + H	2.0e13	0.	0.	est.

^a NIST refers to an average taken from entries in the NIST Chemical Kinetics Database [47].

luminescence. These are listed in the top part of Table 2. Reactions are added here for the new excited state species C₂(*d*): radiative decay ($\tau_{\text{RAD}} = 100$ ns) [34,35], collisional quenching, and potential production steps. In addition, a second expansion of the mechanism (Model C) is considered later. It incorporates kinetics of C₃, C₃H, C₃H₂, and C₂O, including additional possible reactions for producing C₂(*d*). Thermodynamics were taken from the Sandia database [36], except for the coefficients for C₃H obtained from Burcat's compilation [37]. Details of these kinetics are presented later.

Note that the C₂ ground state is $X(^1\Sigma_g^+)$, 1.7 kcal/mol (600 cm^{–1}) more stable than the $a(^3\Pi)$ state measured by the LIF. Judging from kinetic stud-

ies [38] and an arc-jet comparison of C₂(*a*) and C₂(*X*) concentrations [39], rapid equilibration is likely, although reactivities with hydrogen, for example, are different. At flame temperatures above 1200 K, the triplet population is 75% or more of the total, due to its higher degeneracy [40]. Our mechanism considers only a thermal ensemble of the two states, and we choose to interpret the LIF as a ground state probe that detects the majority population.

3. Results

Fig. 1 is an excitation spectrum of the C₂(*d*-*a*) (3, 1) and (2, 0) bands in the rich ethane flame. The prominent bandheads and features from over-

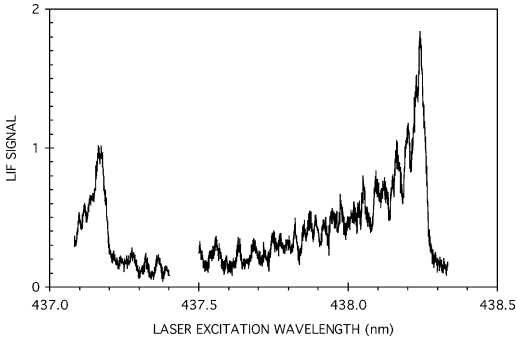
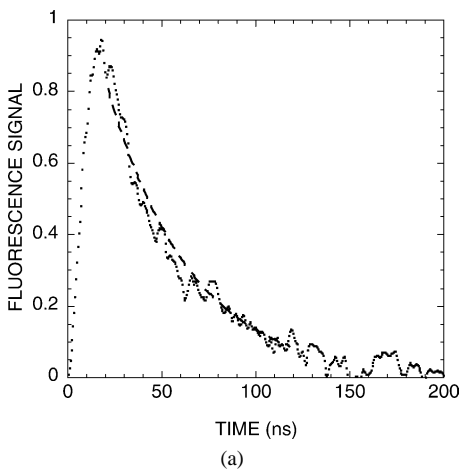


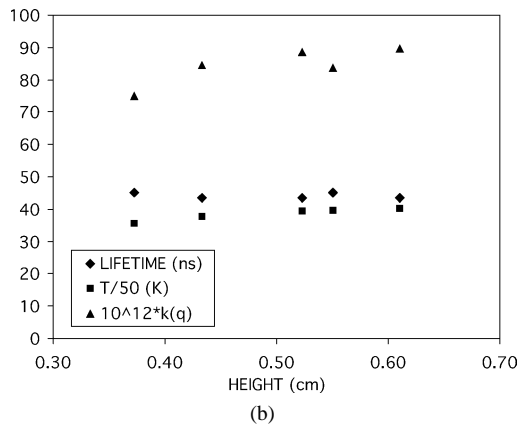
Fig. 1. Laser-induced fluorescence excitation spectrum of $C_2(d-a)$ (3,1) and (2,0) bands excited at its maximum in the rich 30-Torr ethane–air flame. Fluorescence collected in the $\Delta v = 1$ sequence at 473 ± 10 nm. Bands are not to scale. Nominal laser wavelengths given.

lapped lines are apparent and identifiable [1,5,14,35, 41]. Varying the monochromator wavelength reveals weaker fluorescence at the other Swan band Δv sequences. A trace of the LIF signal intensity versus laser power at the bandhead wavelength shows non-linear saturation behavior down to low power. There is also evidence that the signal will continue growing at higher power due to broadening of the overlapped lines. There are some isolated features one can use to attempt unsaturated measurements for an absolute concentration determination, as was done in arc jet experiments [14]. Intensities in the current flame experiment appear too weak for an accurate try without extensive additional effort.

Fluorescence decays were measured at 473 nm for $C_2(d)$ in the five flames at various locations (typically



(a)



(b)

Fig. 2. (a) Fluorescence time decay of $C_2(d-a)$ LIF excited at the (2,0) bandhead at the maximum of the 30-Torr rich methane flame. Dashed line shows the fit to an exponential decay. (b) Flame height dependence of fluorescence decay times (diamonds) (in ns) and quenching rate constants (triangles) (in $10^{-12} \text{ cm}^3/\text{s}$) for $C_2(d-a)$ LIF in the rich methane flame. The measured temperatures (± 50) are also shown (squares). Full scale for the three quantities are 100 ns, 1×10^{-10} , 5000 K. (Legend describes y-axis labels.) The 2σ statistical uncertainties on quenching decays are $\pm 5\%$.

5–7) near the flame front where $C_2(a)$ was present, after exciting at the (2,0) bandhead. The lifetimes, determined by fitting the exponential decays from 90 to 10% of maximum intensity, are constant throughout most of each flame front. Fig. 2a shows a typical data set and fit. Four measurements were also made in the rich ethane flame exciting at the (3,1) bandhead, and gave the same results within experimental error. The different vibronic excited states apparently show nearly identical flame quenching behavior. Use of a single, phenomenological quenching rate for any C_2 LIF excitation or chemiluminescence in a particular flame would appear reasonable, given the spatial and band independence. Table 3 summarizes the lifetime and derived quenching rate constant results for each flame, both at the $C_2(a)$ maximum and for an average of all measurements, where $k_Q = [\tau^{-1} - \tau_{\text{RAD}}^{-1}] (RT/P)$.

Fig. 2b shows the uniformity of lifetimes and derived quenching rate constants throughout the rich methane flame. Note that the C_2 is present only over a fairly narrow temperature range (also shown in the figure), in the flame front. Thus the results are limited as to applicable conditions, but so too apparently are the requirements for data in premixed flames.

We obtained $C_2(d)$ images and $C_2(a)$ height profiles for all five flames, as well as relative maximum signal levels. Fig. 3 shows experimental height profiles in the rich methane flame for CH from Berg et al. [29], for $C_2(d)$ from Smith et al. [6], and for $C_2(a)$ from the LIF experiments of this work. The CH ground state precedes both C_2 distributions, but the precise placement of the $C_2(d)$ chemiluminescent state peak is limited by the low resolution (0.02 cm)

Table 3

 $C_2(d)$ lifetimes (ns) and quenching rate constants (10^{-11} cm³/molec/s) (1σ uncertainties)

Flame	τ at max	Avg τ	k at max	Avg k	% H ₂ O
Rich methane	43.4 ± 0.6	44.1 ± 0.7	8.6	8.3	21.6
St. ethane	49.5 ± 1.4	46.7 ± 1.9	6.95	7.8	18.2
Rich ethane	44.2 ± 2.5	44.0 ± 2.9	7.45	7.5	17.4
St. ethylene	42.2 ± 1.7	41.4 ± 2.4	8.6	8.9	14.9
Rich ethylene	46.0 ± 1.0	44.4 ± 1.4	6.8	7.25	15.4
Avg			7.7 ± 0.8	7.95 ± 0.6	

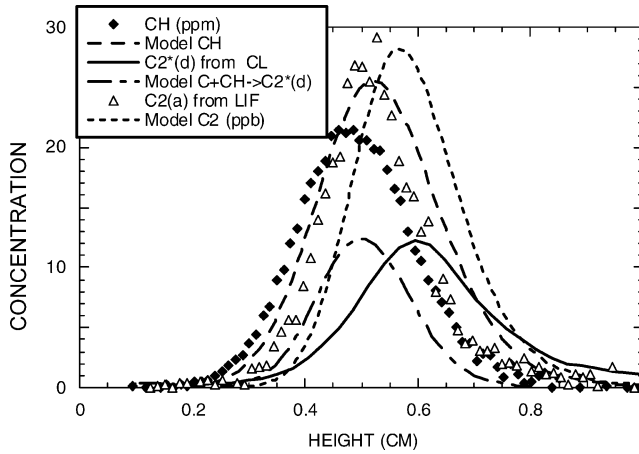


Fig. 3. Experimentally determined height profiles of CH, C₂(a), and C₂(d) in the rich 30-Torr methane–air flame. Initial model results (C + CH for chemiluminescence) are given by the dashed lines. Only the CH model–experiment comparison is on an absolute scale.

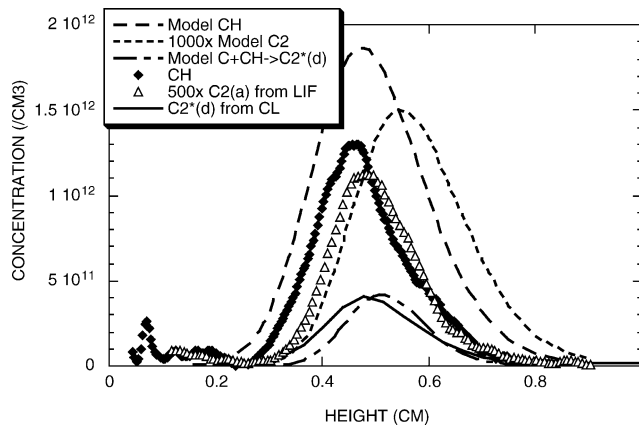


Fig. 4. Experimentally determined height profiles of CH, C₂(a), and C₂(d) in the stoichiometric 25-Torr ethane–air flame. Initial model results (C + CH for chemiluminescence) are given by the dashed lines. Only the CH model–experiment comparison is quantitative.

afforded by the analysis procedure. Model results are also given which are discussed later. Similar profiles were produced in the present study for the other four flames, and plots are presented for the stoichiometric ethane and ethylene flames in Figs. 4 and 5, respectively. Again, CH tends to precede the C₂ species,

at least for the ethane flame, but the separations are small and hard to resolve.

From the relative amounts of chemiluminescence and the calibrated determination of the C₂(d) concentration in the methane flame [6], we derived excited state concentrations for the other flames. By observ-

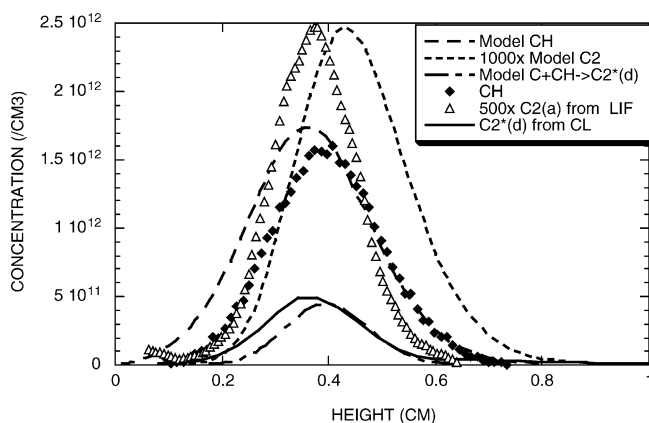


Fig. 5. Experimentally determined height profiles of CH, $C_2(a)$, and $C_2(d)$ in the stoichiometric 25-Torr ethylene-air flame. Initial model results (C + CH for chemiluminescence) are given by the dashed lines. Only the CH model–experiment comparison is quantitative.

Table 4

Maximum concentrations of $C_2(d)$, $C_2(a)$, and CH (cm^{-3})

Flame	$C_2(d)$ (10^6 cm^{-3})	Model A CH + CH ^a	Model B C + CH ₂ ^b	Model C	$C_2(a)$ relative	Model A, B relative	Model C relative	CH (10^{12} cm^{-3})	Model
Rich methane	10.4	15.6	17.2	11.4	1.0			3.4	4.1
St. ethane	4.1	3.2	2.1	1.7	0.6	0.3	0.4	1.3	1.6
Rich ethane	15.6	10.7	12.0	14.3	2.7	1.3	3.3	2.7	3.2
St. ethylene	6.7	2.2	1.4	2.2	1.2	0.3	0.8	1.6	1.4
Rich ethylene	21.6	10.6	11.7	21.7	5.2	2.0	7.5	3.0	3.15
St. methane	1.2	2.4	1.9	1.1				1.5	1.6

^a CH + CH \rightarrow $C_2(d)$, $k = 2.6 \times 10^{-11}$.

^b C + CH₂ \rightarrow $C_2(d)$, $k = 8 \times 10^{-12}$.

ing the relative $C_2(d-a)$ LIF in the different flames at constant laser power, and correcting for minor (measured) quenching rate differences, we also measured the relative ground state amounts, for comparison to mechanism model predictions. (No corrections were made for small differences in populations of the laser-pumped levels at the slightly different peak temperatures.) The peak concentration results are summarized in Table 4. We also determined the CH values shown for the new ethylene and ethane flames from relative LIF intensities, exciting the P₂7 lines of the A-X (0, 0) band at 432 nm and normalizing to the absolute concentration measured previously for the rich methane flame [29].

4. Discussion

In the following we first discuss the chemiluminescence loss process and collisional quenching of $C_2(d)$ as determined from the LIF measurements. Next the chemiluminescence intensities and profiles for methane and then C_2H_x flames are compared with model results using three possible $CH_y + CH_z$ reactions. Rate constants are derived and shortcomings

are noted. Since the LIF measurements also gave relative $C_2(a)$ concentrations, model comparisons with these values and some for CH are discussed. Finally, some suggestions are offered in order to provide an expanded mechanism that corrects for the shortcomings of the model.

4.1. Quenching

The $C_2(d)$ state fluorescence lifetimes and quenching rate constants are similar, within the scatter, for all the hydrocarbon-air low-pressure premixed flames, and are nearly constant throughout the narrow flame front regions where $C_2(a)$ is present and measurements can be made. Quenching is also quite efficient. For the sequence methane, ethane, and ethylene, the fuel carbon content increases while there is a decrease in the amount of the quencher water produced (see the last column of Table 3, from model results). The lack of a significant change in the quenching rate indicates that the quenching efficiency of water is not substantially different from that of the other species. As nitrogen is about 70% of the gas, it likely participates in the quenching. If nitrogen were an inefficient quencher, one would need to assign a very large rate

constant of 2.7×10^{-10} cm³/molec/s to the combined remaining gases.

Our measurements thus suggest a phenomenological rate constant of 8×10^{-11} cm³/molec/s for C₂(*d*) quenching by the flame gases in premixed hydrocarbon–air flames. Previous measurements indicate quenching rate constants by hydrocarbons greater than 1×10^{-10} at room temperature [10,27], and smaller values of approximately 5×10^{-12} for oxygen and xenon [26,28]. Results for a mixture of H₂, H, and Ar in an arc jet at 2200 K show that faster quenching occurs than in our flame, and that $k = 1.6 \times 10^{-10}$ [14]. Thus our large value of the quenching rate constant and the implication that inert nitrogen quenches the fluorescence are not surprising.

4.2. Chemiluminescence kinetics (CH_x)

With the measurement of the C₂(*d-a*) LIF decay rate and thus the chemiluminescence loss rate, we can use the previously determined flame C₂(*d*) concentrations from the chemiluminescence measurements [6] to derive recommended production rate constants. At the peak of the rich CH₄ flame, for example, $1/e$ of the 10.6×10^6 cm⁻³ C₂(*d*) concentration must be formed in each measured decay lifetime of 44 ns. So if $A + B \rightarrow C_2(d)$, $k[A][B] = 2.4 \times 10^{14}$ /cm³/s. Ferguson's carbon isotope labeling work in acetylene flames [20] shows scrambling that indicates an absence of significant preservation of the acetylene C–C bond in *A* and *B*, so these precursors are most likely single carbon species. The exothermic possibilities for source reactions are C + CH, CH + CH, and C + CH₂. At low pressure, the atomic recombination step C + C + M is too slow. Since our flame model adequately predicts the CH profiles and amounts, as shown in Figs. 3–5, it is likely to be accurate in assessing C and CH₂ behavior as well, because their chemistries are closely linked by H and H₂ reactions. Thus the model can be reliably used to evaluate the possible C₂(*d*) production kinetics.

From the rich methane flame results only, and using our limited extended version of GRI-Mech 3.0 [6], the candidate reactions are: C + CH at 2×10^{-11} , CH + CH at 1.8×10^{-11} , and C + CH₂ at 5×10^{-12} cm³/molec/s. Any one of the three will predict the measured intensity, as would any fractional mixture of the rate constants that adds to one. If the data clearly showed C₂(*d*) chemiluminescence peaking later in the flame than CH LIF, it would support the first reaction according to model comparisons, as C is produced after CH in the flame chemistry. However it is difficult to obtain precise spatial resolution in comparing the two experiments. While the model performs reasonably well in predicting the peak positions and widths in the rich methane flame (uniformly

a little late), for the stoichiometric ethane and ethylene flames the model provides late-predicted C₂ LIF peaks, especially relative to the CH peak. (This tardiness is pronounced for all species profiles in the rich flames, which are not shown.) Spatial resolution in the low-pressure flames is not sufficient to definitively select the Swan band chemiluminescence production reaction. The model traces shown in Figs. 3–5, for the C + CH reaction, are only 0.2 cm higher above the burner than those for the two other possible chemiluminescence reactions.

Discharge flow reactor results [19], some previous flame correlations [21,41], and shock tube study results [23] provide arguments that suggest that CH + CH is not the Swan band emission source. If C + CH is the Swan band emission source, a high rate constant would be required to fit our results, and this would imply an abnormally high product branching fraction to excited state C₂ (and prospects for a Swan band visible chemical laser). Given the large rate required for the CH reactions, a bias in favor of the smallest fraction of the collision rate that leads to excited states would suggest C + CH₂ as the source reaction.

The ethane and ethylene flames provide additional data to derive the C₂(*d*) production reaction and rate constant, and an opportunity to validate the full chemiluminescence mechanism for other hydrocarbon flames. Applying the model just developed for the methane combustion optical emissions, C₂(*d*) chemiluminescence is underpredicted for the other rich flames by roughly half. However, this model does approximately predict the measured ground state CH levels, as shown in the last two columns of Table 4, and by inference, model values for possible C and CH₂ precursors of C₂(*d*) should also be accurate as they are closely related by the simple reactions $H + CH_x \leftrightarrow H_2 + CH_{x-1}$. So this underprediction is unexpected. If we average the C + CH₂ rate constants derived from the three rich flames using the GRI-Mech 3.0 chemistry, $k = 1.0 \times 10^{-11}$ cm³/molec/s, rather than the 0.5 value from the rich CH₄ flame alone. Larger than expected (50%) error bounds ensue. (If C + CH were responsible, the averaged $k = 3.8 \times 10^{-11}$; for CH + CH as the sole source, $k = 3.6 \times 10^{-11}$. The proportional increases over the rich methane flame results are similar.)

The observed visible emissions from the C₂H_x stoichiometric flames are significantly underpredicted by factors of 2–4 by the model C₂(*d*) concentrations using the larger C + CH₂ or CH rate constants from the above averaging. The CH + CH step accounts for the equivalence ratio dependence better. The observed ratio of C₂^{*}(*d*) from the rich ethane flame to that from stoichiometric ethane flame is 4, while the model predicts ratios of 8, 6, and 3 respectively for the potential production reactions C + CH, C + CH₂, and

CH + CH. For ethylene the measured $C_2^*(d)$ ratio for rich versus stoichiometric flames is 3, while the model predicts ratios of 10, 8, and 5 for the three possible reactions. Thus the stoichiometry dependence suggests CH + CH is the most likely source reaction for $C_2(d)$, and does not favor the reaction C + CH as the source. The predicted sensitivity of the $C_2(d)$ ratios for C_2H_x flames relative to the CH_4 flame depends much less on the choice of production reaction. A final comparison is provided by the dependence of the Swan band chemiluminescence on the equivalence ratio for the two methane flames. This dependence is predicted well, with better agreement for the reactions C + CH_2 or C + CH than for CH + CH. These modeling difficulties for Swan band emissions in C-2 fuels, especially for stoichiometric flames, suggest additional chemistry needs to be considered.

We can recommend a third rate constant that is based on all the methane and ethane flame measurements, instead of only the methane or the rich flame measurements. The full $C_2(d)$ data for the methane and ethane flames are best fit (although still with 33% deviations) by $k = 2.6 \times 10^{-11}$ for CH + CH \rightarrow $C_2(d)$ + H_2 (Model A) or by $k = 8 \times 10^{-12}$ for C + $CH_2 \rightarrow C_2(d)$ + H_2 (Model B). See columns 3 and 4 of Table 4. For the ethylene flames the predicted values were consistently less than the experiments, and the difference exceeds 50%. This may be attributable to the fact that GRI-Mech 3.0 was not optimized with respect to ethylene fuel targets. Although the predictions using CH + CH (Model A) are slightly better, given the other experimental evidence against the CH + CH reaction and the imperfect fits of the data, the C + CH_2 rate constant choice (Model B) is recommended for modeling when GRI-Mech 3.0 is not extended to include C_3 kinetics. Ways to improve the poor fits are discussed in Section 4.4.

4.3. C_2 kinetics

The relative amounts of $C_2(a)$ measured by LIF in the different flames is a test of the C_2 and C_2H kinetics in the mechanism. These kinetics must be modeled correctly to develop an accurate model of CH(A) chemiluminescence, which is formed from these precursors. The results in Table 4 show that $C_2(a)$ is systematically underpredicted in the C_2H_x flames by a factor of 2 relative to the CH_4 flame. Some discrepancies for the ethylene flames might be expected considering that GRI-Mech was not optimized to any ethylene flame property targets [33]. We compared C_2 sensitivities from the rich ethane and methane flame calculations, to determine which uncertain rate constants might be altered to correct this relative underprediction, keeping in mind that changes in the fairly well-predicted CH(A) levels in

these flames are unwelcome. Significant sensitivity differences (C_2 vs CH(A)) were seen for C + $O_2 \rightarrow$ CO + O, $C_2 + H_2 = C_2H + H$, C + CH = $C_2 + H$, and $C_2 + O_2 \rightarrow 2CO$, but the values were only ~ 0.2 , which indicates that several factor-of-2 modifications of rate constants would be required to begin significantly addressing the relative C_2 underprediction.

The $C_2(a)$ profile and its position relative to CH are well predicted for the rich methane flame (see Fig. 3). Although an absolute concentration would test the C_2 kinetics better, low concentrations and signal levels plus spectral complexity restricted the current LIF observations to conditions of optical saturation for the transition. While any quantitative interpretation of the partly saturated bandhead intensity is imprecise, signal levels are near those expected for the model $C_2(a)$ predictions of 20 ppb. However, in both stoichiometric ethane and ethylene flames, the predicted $C_2(a)$ profile occurs later than in the experiment. Coupled with the underprediction of relative concentrations by the model, this suggests that larger production rates from other reactions are required in the mechanism from C_2H_x fuels.

4.4. Expanded mechanism

An attempt was made to expand and improve the kinetics mechanism for C_2 prediction by adding the kinetics of C_3 and related species to develop model C. The poor predictions shown above when results from all flames were used to derive the production rate constant demonstrate that additional chemistry must be included. More work will be needed to develop an acceptable set of rate constants. The last section of Table 2 provides the additions we considered. Both C and CH have been measured to react rapidly with acetylene, so this is included as a path to C_3H_x . The added chemistry in Table 2 considers the resulting C_3 and C_3H products as potential alternate routes to forming C_2 and C_2^* by reaction with O atoms. We seek improved predictions for the fuel and stoichiometry dependences for both C_2 states. The kinetics additions to GRI-Mech 3.0 are given with sources [42–47] in Table 2. The last section in the table provides the expanded C_3 mechanism, and follows the additions from our previous work and the reported $C_2(d-a)$ chemiluminescence rates. Many of the new rate constants are necessarily estimated, and generally our C_3H_x loss rates are somewhat larger and our formation rates smaller than one might ordinarily choose, in part to avoid perturbing the original GRI-Mech 3.0 predictions of measured CH concentrations.

Kruse and Roth have reported some high-temperature shock tube rate constants involving C_2 [48,49]. Extrapolating down to flame temperatures, their rate for $C_2 + O_2$ is about twice the number from the lit-

Table 5

Isotopic acetylene flame results [20]: isotopomer fractions in the fuel, observed Swan band emissions, and four model predictions

CC isotope	Fuel	$C_2(d-a)$	Random (C-1)	Original (C-2) (Model A, B)	New (C-3)	1:1 Avg C-1 and C-3 (Model C)
12-12	0.689	0.617	0.60	0.69	0.65	0.62
12-13	0.164	0.323	0.35	0.16	0.25	0.30
13-13	0.147	0.060	0.05	0.15	0.10	0.07

erature that we chose [48]. Our estimate for $O + C_2$ is four times their value [49]. The GRI-Mech rate constant for $C_2H + H_2$ is 2.5 times their value [48], and a similar factor applies to the value we chose for $C_2 + H_2$. Using these other kinetics will increase the predicted variation of C_2 with stoichiometry. In addition to overpredicting this variation, the faster added chemistry would begin to alter some GRI-Mech predictions regarding CH and CH(A). A recent arc jet mechanism [15] can be used to estimate the rate constants for many rapid C_3H_x reactions, but no oxygen reactions are included in these kinetics.

The additions to the mechanism roughly double or triple the $C_2(a)$ concentrations, through the C_3 pathway mentioned above. In Table 4, the results labeled Model C show that the new kinetic mechanism has corrected the underprediction of the fuel dependence of observed $C_2(a)$ concentrations, although it now somewhat overpredicts the variations caused by changing the stoichiometry. These ratios, and some absolute concentration determinations, could be used to fine-tune the still uncertain critical kinetics controlling the C_2 concentrations. More work is required to produce a thorough, complete, and evaluated set of C_3H_x kinetics for inclusion. It is clear that these changes were necessary to remove the poor accounting for the C_2 variations observed among the various flames, and that the sequence $C + C_2H_2 \rightarrow C_3H + H \rightarrow C_3 + H_2$, $C_3 + O \rightarrow C_2 + CO$ is important. Interestingly, the C_2H concentration and hence the predicted CH(A-X) chemiluminescence (from $C_2H + O$ or O_2) are not significantly altered by the added kinetics at the rates chosen. They remain closely connected to the acetylene kinetics.

Next we look at improving the Swan band predictions. Changes made to the chemiluminescence mechanism operate independently of the above, as only concentrations of C_2 and the newly added species have changed as a result of this specific mechanism expansion. To predict better the fuel dependence for $C_2(d)$, we need an additional source reaction. Two possibilities were considered. The revised mechanism (C) predicts partial equilibrium amounts of C_2O around 10 ppm, so a fast $C + C_2O \rightarrow CO + C_2(d)$ rate constant, similar in size to that proposed for $C + CH$ earlier, could make a significant contribution. This reaction is known to form vibrationally excited $C_2(d)$

in $v' = 6$ [25]. While spectra that we obtained from our flame emissions do show such excited level populations, they do not predominate. We focus instead on an alternative reaction known to yield Swan band emissions, and with reactants present in high concentrations, $O + C_3$. Given that C_3 is formed following the $C + C_2H_2$ reaction, we can expect increased Swan band emission yields for the C_2H_x fuels compared with methane due to the inclusion of this additional chemiluminescent reaction source.

Ferguson's isotope work shows considerable scrambling of carbon-carbon bonds prior to Swan band emission [20], and implications of a $O + C_3$ source must be considered. Table 5 gives the carbon isotope distributions of the acetylene fuel and for the measured $C_2(d-a)$ emissions from Ferguson's second flame, where the first row of data provides the fractions for $^{12}C^{12}CH_2$ and $^{12}C^{12}C(d-a)$. The last four columns in Table 5 provide the expected values for the cases of random scrambling (single CH_x fragment sources, such as $C + CH_2$, labeled C-1), for retention of the carbon bond structure (a C_2H_x or polymer source, labeled C-2), for a $C + C_2X$ mechanism ($C + C_2O$ or $C + C_2H_2$ plus $O + C_3$, labeled C-3), and for an average of $C + CH_2$ and $O + C_3$. It would appear from the data that 25–50% of the C_2^* emission could be due to the latter reaction. We examined the maximum alternative by adjusting the two rate constants so each pathway contributes half the source term for $C_2(d)$ in the rich methane flame model. The $C + CH_2$ rate becomes $4 \times 10^{-12} \text{ cm}^3/\text{molec/s}$, which is half of its previous value.

The results for $C_2(d)$ are summarized in Table 4 in the column denoted Model C. The rate constants of Table 2 were used. Excellent agreement is now obtained for the rich flames regardless of fuel. A lesser contribution from the $O + C_3$ reaction would begin to degrade the agreement. Good predictions are obtained for the near-stoichiometric methane flame, although the stoichiometric ethane and ethylene Swan band intensities remain underpredicted. Since C_3 formation is highly favored as the mixture becomes fuel-rich, it is not surprising that adding this mechanism failed to improve this problem. We also examined the dispersed visible emission spectra for the stoichiometric flames, looking for experimental evidence that another excited species might contaminate the

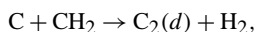
leaner flame visible emission intensities, but found none. Since bright visible Swan band emissions and their diagnostic use are likely only under fuel-rich conditions, the kinetic error symptomized by modeling difficulties near equivalent stoichiometries should have a minimal effect. We also note that the recommended value of $k = 7 \times 10^{-13} \text{ cm}^3/\text{molec/s}$ for $\text{O} + \text{C}_3 \rightarrow \text{C}_2(d) + \text{CO}$ is less than 1% of the total estimated rate constant for these reactants.

5. Conclusions

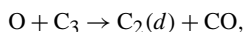
Profiles, concentrations, and quenching rates have been determined for $\text{C}_2(d)$ and $\text{C}_2(a)$ by measuring Swan band chemiluminescence and (2, 0) LIF. A general flame quenching rate constant of $8 \times 10^{-11} \text{ cm}^3/\text{molec/s}$ is recommended for $\text{C}_2(d) + \text{M} \rightarrow \text{C}_2(a) + \text{M}$ (or other products). Within the scatter of the measurements, no trends dependent on composition (including water) were seen. An optimum production rate constant for use with GRI-Mech 3.0 and our small set of added chemiluminescence kinetics (Model B) is $\text{C} + \text{CH}_2 \rightarrow \text{C}_2(a) + \text{H}_2$, $k = 8 \times 10^{-12} \text{ cm}^3/\text{molec/s}$. Alternately, for rich stoichiometries only, one may use $\text{C} + \text{CH}_2$ at 1×10^{-11} , $\text{C} + \text{CH}$ at 4×10^{-11} , $\text{CH} + \text{CH}$ at 3.5×10^{-11} , or any weighted combination of the three. In most rich combustion modeling situations, little significant operational difference is expected, due to close coupling of the CH_x species via reactions with abundant H and H_2 . Model B, however, presents significant uncertainty with respect to predicting Swan band emission variations with fuel and stoichiometry.

Relative $\text{C}_2(a)$ concentrations determined from the measurements disagree with the model predictions by a factor of 2. This suggests some need for improved modeling of reactions involving C and C_2 , but one should be careful not to change the current predictions of CH and CH(A), which are adequate. An extended model (Model C) was introduced that includes the kinetics of C_3 , its formation via $\text{C} + \text{C}_2\text{H}_2$, and the production of ground and excited state C_2 by its reaction with O. This greatly improves the model results for the relative amounts of $\text{C}_2(a)$ observed in the various flames and for the dependence of the chemiluminescence on the fuel. However, further improvements of the kinetics are needed.

Recommended rate constants with the enlarged mechanism (Model C) are:



$$k = 4 \times 10^{-12} \text{ cm}^3/\text{molec/s},$$



$$k = 7 \times 10^{-13} \text{ cm}^3/\text{molec/s}.$$

Acknowledgments

This research was supported by the NASA Microgravity Program, Contract NAS3-99143. J. Schneiderman's summer research was sponsored by an NSF Research Experiences for Undergraduates Program at SRI.

References

- [1] A.G. Gaydon, *The Spectroscopy of Flames*, second ed., Chapman & Hall, London, 1974.
- [2] J.D. Shea, *Phys. Rev.* 30 (1927) 825–843.
- [3] C. Arpigny, *Astrophys. J.* 144 (1966) 424–427.
- [4] R. Gredel, E.F. van Dishoeck, J.H. Black, *Astrophys. J.* 338 (1989) 1047–1070.
- [5] W.H. Smith, *Astrophys. J.* 156 (1969) 791–794.
- [6] G.P. Smith, J. Luque, C. Park, J.B. Jeffries, D.R. Crosley, *Combust. Flame* 131 (2002) 59–69.
- [7] C.R. Shaddix, K.C. Smyth, *Combust. Flame* 107 (1996) 418–452.
- [8] Y. Ikeda, J. Kojima, T. Nakajima, F. Akamatsu, M. Katsuki, *Proc. Combust. Inst.* 28 (2000) 343–350.
- [9] K.H. Becker, D. Haaks, T. Tatartzyk, *Z. Naturforsch.* A 29 (1974) 829–830.
- [10] J.E.M. Goldsmith, D.T.B. Kearsley, *Appl. Phys. B* 50 (1990) 371–379.
- [11] B.A. Williams, L. Pasternack, *Combust. Flame* 111 (1997) 87–110.
- [12] C. Kamanski, P. Ewart, *Appl. Phys. B* 61 (1995) 585–592.
- [13] R.J.H. Klein-Douwel, J.J.L. Spaanjaars, J.J. ter Meulen, *J. Appl. Phys.* 78 (1995) 2086.
- [14] J. Luque, W. Juchmann, J.B. Jeffries, *J. Appl. Phys.* 82 (1997) 2072–2081.
- [15] Yu.A. Mankelevich, N.V. Suetin, M.N.R. Ashfold, W.E. Boxford, A.J. Orr-Ewing, J.A. Smith, J.B. Wills, *Dia. Rel. Mater.* 12 (2003) 383–390.
- [16] J.B. Wills, J.A. Smith, W.E. Boxford, J.M.F. Elks, M.N.R. Ashfold, A.J. Orr-Ewing, *J. Appl. Phys.* 92 (2002) 4213.
- [17] X. Mercier, E. Therssen, J.R. Pauwels, P. Desgroux, *Proc. Combust. Inst.* 30 (2004), 2D07.
- [18] A. Staicu, R.L. Stolk, J.J. ter Muelen, *J. Appl. Phys.* 91 (2002) 969.
- [19] J. Grebe, K.H. Homann, *Ber. Bunsenges. Phys. Chem.* 86 (1982) 587–597.
- [20] R.E. Ferguson, *J. Chem. Phys.* 23 (1955) 2085–2089.
- [21] E.M. Bulewicz, P.J. Padley, R.E. Smith, *Proc. R. Soc. A* 315 (1970) 129–148.
- [22] A. Bergeat, T. Calvo, G. Dorthe, J.-C. Loison, *J. Phys. Chem. A* 103 (1999) 6360–6365.
- [23] C.T. Bowman, D.J. Seery, *Combust. Flame* 12 (1968) 611–614.
- [24] M.I. Savaditti, H.P. Broida, *J. Chem. Phys.* 45 (1966) 2390–2396.
- [25] C. Kunz, P. Harteck, S. Dondes, *J. Chem. Phys.* 67 (1967) 4157–4158.
- [26] H. Okabe, R.J. Cody, J.E. Allen Jr., *Chem. Phys.* 92 (1985) 67–73.

- [27] G.A. Raiche, D.R. Crosley, R.A. Copeland, Resonance enhanced multiphoton photodissociation of C_2H_2 , in: Western States Section Combustion Institute, Fall 1989 Meeting, Livermore, CA, 1989, Paper 89-47.
- [28] M. Castilleja, J.M. Figuera, M. Martin, *Chem. Phys. Lett.* 107 (1984) 561.
- [29] P.A. Berg, D.A. Hill, A.R. Noble, G.P. Smith, J.B. Jeffries, D.R. Crosley, *Combust. Flame* 121 (2000) 223–235.
- [30] J. Luque, D.R. Crosley, *Appl. Phys. B* 63 (1996) 91.
- [31] W. Bischel, D.J. Bamford, L.E. Jusinski, *Appl. Opt.* 25 (1986) 1215.
- [32] R.J. Kee, J.F. Grcar, M.D. Smooke, J.A. Miller, A Fortran Program for Modeling Steady Laminar One-Dimensional Premixed Flames, Sandia Report SAND85-8240, 1985.
- [33] G.P. Smith, D.M. Golden, M. Frenklach, N.W. Moriarty, B. Eiteneer, M. Goldenberg, C.T. Bowman, R.K. Hanson, S. Song, W.C. Gardiner, V. Lissianski, Z. Qin, GRI-Mech 3.0 Web site, http://www.me.berkeley.edu/gri_mech/, 1999.
- [34] C. Naulin, M. Costes, C. Dorthe, *Chem. Phys. Lett.* 143 (1988) 496–500.
- [35] R.S. Urdahl, Y. Bao, W.M. Jackson, *Chem. Phys. Lett.* 152 (1988) 485–490.
- [36] R.J. Kee, F.M. Rupley, J.A. Miller, Chemkin Thermodynamic Data Base, Sandia Report 87-8215B, 1987.
- [37] A. Burcat, B. McBride, Ideal Gas Thermodynamic Data for Combustion and Air Pollution Use, Technion Report TAE 697, 1994.
- [38] S.L. Baughcum, R.C. Oldenborg, *Am. Chem. Soc. Symp.* 249 (1984) 257–266.
- [39] C.J. Rennick, J.A. Smith, M.N.R. Ashfold, A.J. Orr-Ewing, *Chem. Phys. Lett.* 383 (2004) 518–522.
- [40] M.W. Chase, C.A. Davies, J.R. Downey, D.J. Frurip, R.A. McDonald, A.N. Syverud, *J. Phys. Chem. Ref. Data* 14 (Suppl. 1) (1985) 646.
- [41] R. Bleekrode, W.C. Nieuwpoort, *J. Chem. Phys.* 43 (1965) 3680–3687.
- [42] N. Haider, D. Husain, *Z. Phys. Chem.* 176 (1992) 133–150.
- [43] R. Guadagnini, G.C. Schatz, S.P. Walch, *J. Phys. Chem. A* 102 (1998) 5857–5866.
- [44] H.H. Nelson, H. Helvajian, L. Pasternack, J.R. McDonald, *Chem. Phys.* 73 (1993) 431.
- [45] M.W. Marcus, P.P. Roth, *Int. J. Chem. Kinet.* 24 (1992) 433–445.
- [46] W. Bauer, K.H. Becker, R. Meuser, *Ber. Bunsenges. Phys. Chem.* 89 (1985) 340.
- [47] W.G. Mallard, F. Westley, J.T. Herron, R.F. Hampson, D.H. Frizzell, NIST Chemical Kinetics Database, NIST Standard Reference Database 17, Version 7.0, 2000.
- [48] T. Kruse, P. Roth, *J. Phys. Chem. A* 101 (1997) 2138–2146.
- [49] T. Kruse, P. Roth, *Proc. Combust. Inst.* 27 (1998) 193–200.